Physics-Informed Orbit Determination for Cislunar Space Applications

Andrea Scorsoglio, Andrea D'Ambrosio, Luca Ghilardi, Roberto Furfaro
Department of Systems & Industrial Engineering, The University of Arizona
Vishnu Reddy
Lunar and Planetary Laboratory, The University of Arizona

ABSTRACT

Accurate orbit determination is critical for cislunar space monitoring. The traditional techniques used for OD in Low Earth Orbits (LEO) may not work effectively in cislunar space, therefore there is a need for new methods to estimate the state of a maneuvering target in such environment. The paper proposes a new approach utilizing Physics Informed Neural Networks (PINN), a unique type of neural network designed for solving forward and inverse problems governed by parametric differential equations. The OD problem is treated as a dynamical problem where the aim is to solve the governing differential equations starting from the observation data. The system is capable of estimating the target's state using passive angle-only observations, without requiring any initial guess or integration. If a maneuvering target is considered, including the maneuvers as unknown dynamical components in the equations of motion, allows the system to estimate both the state of the target and the maneuvers themselves at any time within the observation span. The method is tested on both real angle-only observations of cislunar objects provided by the Space4 Center, and synthetically generated data. The paper concludes that the proposed method has the potential to improve OD accuracy in cislunar space and could be a promising alternative to traditional methods.

1. INTRODUCTION

Since the beginning of space exploration, determining the orbit of a spacecraft, known as orbit determination (OD), has been a critical issue. The success of every mission hinges on accurately estimating the spacecraft's state at any given time. This reliable and precise state estimation is crucial for planning necessary adjustments and tasks, such as station-keeping and correction maneuvers, as well as missions involving relative motion, like rendezvous and docking. In recent years, there has been a growing interest in OD in the cislunar space [1], as the Moon becomes a target for both human and robotic exploration [2]. Specifically, with the Lunar Orbital Platform-Gateway's [3] development as a lunar outpost orbiting one of the Lagrangian points in the Earth-Moon system, there has been renewed attention on OD in the cislunar space.

When conducting missions in Low Earth Orbits (LEO), state estimation measurements can be obtained from multiple sources and are generally straightforward to acquire, such as using onboard Global Positioning System (GPS) or ground-based observations. There are two commonly used techniques for Orbit Determination (OD): Initial Orbit Determination (IOD) and statistical estimation methods. IOD methods [4], including Gauss' Method, Double-R Iteration, or Gooding's Method, only require a small set of angular measurements to estimate an orbit. In contrast, statistical orbit determination methods [5] rely on a larger collection of measurements to refine the estimate and can be categorized into batch algorithms (commonly referred to as least squares) or sequential algorithms (such as the Kalman filter and its variants), which estimate the initial state and current state in real time, respectively. These methods are interdependent and typically require a track initialization using IOD methods, followed by batch least squares, and finally an online orbit determination method using the solution from the previous step as an initial reference trajectory. However, implementing this procedure for objects in cislunar space is challenging and requires a thorough understanding of measurement quality.

The application of standard space traffic management techniques to objects in cislunar space has been found to produce inadequate results or be unusable altogether. In the past, spacecraft traveling towards the Moon have typically used a combination of ground-based initial state updates and inertial measurements. Although these methods are effective, they are prone to error drift caused by numerical integration. For cooperative objects in cislunar space, such as the

ARTEMIS spacecrafts, orbit determination is now achieved using a batch least-squares method that analyzes range and Doppler tracking measurements obtained from the NASA Deed Space Network (DSN). This method is also employed for tracking deep-space satellites, including those located further away from the Moon. Despite its ability to reduce estimation error to less than 0.1 km and 0.1 cm/s for position and velocity, respectively, this method cannot be utilized for non-cooperative objects. In such cases, orbit determination can only be accomplished through optical observations. However, for cislunar objects whose dynamics is chaotic, most orbit determination techniques can only provide state estimates for short periods close to the observation time. Additionally, if the non-cooperative object is an artificial satellite, orbit determination is nearly impossible due to the need for frequent station-keeping maneuvers that cannot be accounted for in the OD process unless they are known, further degrading its capabilities.

The objective of this paper is to perform orbit determination in cislunar space using angle only observations in a restricted perturbed two body problem framework. Our approach utilizes Physics Informed Neural Networks (PINN), a unique type of neural network designed for solving forward and inverse problems governed by parametric differential equations. To address the OD problem, we treat it as a dynamical problem and aim to estimate the solution of the governing differential equations based on observation data. To achieve this, we use a neural network to approximate the solution of the system of differential equations, which is trained by incorporating the dynamical model into the neural network's loss function as a regularizer. This ensures that the network's training is penalized when the physics of the problem is violated. By including the maneuvers as unknown dynamical components in the equations of motion, the system is capable of estimating both the state of a maneuvering target and the maneuvers themselves at any time within the observation span using passive angle-only observations, without requiring any initial guess or integration. The method has been introduced in some previous works by the authors, where it was applied to simulated data, both in keplerian [6] and non-keplerian dynamics [7, 8], and real observation data of some GEO satellites and the heliocentric object 2020SO obtained from telescopes at the Space4 Center located in Tucson., Arizona [9]. The current work focuses on applications to the real observation data obtained from the Space4 Center and other observatories of the upper stage of the Chang'e 5 spacecraft (that was demonstrated to have hit the far side of the Moon on 4 March 2022). Moreover, the method is tested on a simulated trajectory obtained by adding a maneuver, starting from the data mentioned above. This work showcases improved capabilities of the method in predicting the impact with the Moon and maneuver estimation.

2. METHODOLOGY

The aim of the paper is to showcase the capabilities of a novel method called Physics Informed Orbit Determination (PIOD) [8] for orbit determination on non-cooperative objects moving in cislunar space. The method leverages an accurate dynamical model and physics informed neural networks (PINN), which are introduced in this section.

2.1 Physics Informed Orbit Determination

Physics informed neural networks exploit a neural network (NN) to approximate a certain quantity by using the physics of the problem to regularize the network training. In this case the goal is to approximate the state of the system $\mathbf{x}_{NN} = [\mathbf{r}_{NN}, \mathbf{v}_{NN}]$, in terms of position $\mathbf{r}_{NN} = [x, y, z]$ and velocity $\mathbf{v}_{NN} = [\dot{x}, \dot{y}, \dot{z}]$, as a function of time.

Consider a problem with governing equations in the following form:

$$\dot{\mathbf{x}} = f(\mathbf{x}) \tag{1}$$

The NN approximates the state at predetermined discretization points (i.e., time instants). These are used to build the loss vector ($\mathscr{L}$), which is made up of the residuals ($\boldsymbol{L}_\theta$) between the available observations and the corresponding values predicted by the NN, and the residuals of the ODEs ($\boldsymbol{L}_f$) describing the physics of the problem at each discretization point (see Eq. (8)). Specifically, the losses can be written as:

$$\boldsymbol{L}_f = f(\mathbf{x}) \tag{2}$$

$$\boldsymbol{L}_\theta = \tilde{\boldsymbol{\theta}} - \boldsymbol{\theta}_{NN} \tag{3}$$

where $\boldsymbol{\theta} = [\sin\alpha, \cos\alpha, \sin\delta]^T$ is the vector associated with the observables at each time instant the observations are available, and the subscript *NN* indicates those terms estimated through the NN.

The vector $\tilde{\boldsymbol{\theta}}$ contains the actual real observations (RA and DEC) coming from the telescope images after the astrometry pipeline is applied. The total loss vector is then defined as:

$$\mathscr{L} = \begin{bmatrix} \lambda_f \boldsymbol{L}_f \\ \lambda_\theta \boldsymbol{L}_\theta \end{bmatrix} \tag{4}$$

with λ_f and λ_θ being the weights associated with the two loss terms. These weights are introduced to be able to prioritize physics or data depending on the confidence level on the physics model or the observation data. For example, if the level of confidence is higher on the acquired data, λ_θ should be greater than λ_f. Conversely, if the data is noisy or not accurate, the physics should be trusted more, which means $\lambda_f > \lambda_\theta$.

These coefficients can also be used selectively decrease the contribution to the final solution of outliers (e.g., when unexpected light sources affect the images taken by the telescopes with the consequence of unreliable astrometry). The values of λ_f and λ_θ should be carefully set according to the order of magnitude of the loss terms. As a final remark on the total loss vector in Eq. (4), the length of the vector $\boldsymbol{L}_f$ (N_f) is generally different from the length of $\boldsymbol{L}_\theta$ (N_θ), since we would like to satisfy the physics constraints also in time instants where the observations are not available. This is crucial to solve the OD problem especially when a limited number of observations is available. The parameters of the network can in general be optimized either considering the loss function as a vector or taking the mean squared error (MSE). In this case, we use the MSE ($\mathscr{L}_{MSE} = MSE(\mathscr{L})$). The learned parameters are then used to recover the solution at any time within the selected time span.

In this work, single layer PINN trained via Extreme Learning Machine algorithm [10] are employed. According to the ELM formalism, the input weights (**w**) and biases (**b**) of the NN can be set randomly and kept fixed during training. The only parameters that are learnt are the output weights $\boldsymbol{\beta}$.

Selecting an ELM as NN allows to use a least-square procedure to compute the optimal parameters [11], instead of the more common gradient-based algorithms, which allows for faster training times. Consider a generic function ($g_j(z)$), it is approximated via ELM through the following relation:

$$g_j(z) = \sum_{q=1}^{L} \beta_{j,q} \sigma\left(w_q z + b_q\right) = \boldsymbol{\sigma}^T(z) \boldsymbol{\beta}_j \tag{5}$$

where z is the input variable; w_q, b_q, and $\beta_{j,q}$ are the input weight, bias and output weight associated with the q-th neuron; σ is the activation function, and L is the total number of neurons.

In the proposed PIOD framework, the discretized time is the input of the NN. However, the time domain is usually mapped in [-1,1], since activation functions work better in such interval. The outputs of the network are the three components of the position, each associated with its own set of output weights ($\boldsymbol{\beta}_x$, $\boldsymbol{\beta}_y$, and $\boldsymbol{\beta}_z$). The vector of the unknown is:

$$\boldsymbol{\beta}_1 = [\boldsymbol{\beta}_x, \boldsymbol{\beta}_y, \boldsymbol{\beta}_z] \tag{6}$$

In this work we also develop a network that can estimate position and control acceleration. If the acceleration is to be estimated, the vector of unknowns becomes:

$$\boldsymbol{\beta}_2 = [\boldsymbol{\beta}_1, \boldsymbol{\beta}_{u_x}, \boldsymbol{\beta}_{u_y}, \boldsymbol{\beta}_{u_z}] \tag{7}$$

where $[u_x, u_y, u_z]$ is the control acceleration with components in all the directions. The acceleration components in this case are estimated directly as scalar values at each time step within the optimization method instead of being expanded through the network. The analytical expression of the Jacobian of the losses with respect to each vector of unknown ($\mathbf{J} = \frac{\partial \mathscr{L}}{\partial \boldsymbol{\beta}}$) has been calculated in order to speed up training. This can be done by hand or by means of symbolic toolboxes and automatic differentiation techniques. In this case, it has been made possible by the open source Matlab package Adigator [12].

2.2 Dynamical model

An accurate definition of the equations of motion is pivotal for training PINN effectively using real data. The model employed in this work is the perturbed two-body model written in terms of Cartesian coordinates. In the following, all the vectors are meant to be expressed in the Earth-Centered-Inertial (ECI) J2000 reference frame. The system of

ordinary differential equations (ODEs) governing the motion in this framework, with the time being the independent variable, is:

$$\begin{cases} \dot{\mathbf{r}} = \mathbf{v} \\ \dot{\mathbf{v}} = -\frac{\mu_e}{r^3}\mathbf{r} + \mathbf{a}_p + \mathbf{u} \end{cases} \tag{8}$$

where $\mathbf{r}(t) = [x, y, z]$ and $\mathbf{v}(t) = [\dot{x}, \dot{y}, \dot{z}]$ are the position and velocity vector of the satellite with respect to the center of the Earth, $\mathbf{a}_p$ is the vector containing all the perturbing accelerations, and $\mathbf{u}$ is the control acceleration vector. Moreover, $\mu_e = 398600.1$ km^3/s^2 is the Earth gravitational constant and r is the magnitude of the position vector, i.e., $r = ||\mathbf{r}||$. The control acceleration vector can be expressed as:

$$\mathbf{u} = [u_x, u_y, u_z] \tag{9}$$

representing the control acceleration in the ECI frame.

The perturbing acceleration comprises the following contributions: zonal harmonics up to J_6 and tesseral harmonic J_{22} for the Earth gravitational field; Sun, Moon, and Mars third body perturbation accelerations. While the explicit expressions of the perturbing accelerations associated with the Earth gravitational field are provided in the references [9], the perturbation acceleration of the generic *i*-th third-body can be written as follows:

$$\mathbf{a}_{3B_i} = \mu_{3B_i}\left(\frac{\mathbf{r}_{sat-3B_i}}{r^3_{sat-3B_i}} - \frac{\mathbf{r}_{e-3B_i}}{r^3_{e-3B_i}}\right) \tag{10}$$

where μ_{3B} is the gravitational constant related to the third body, $\mathbf{r}_{sat-3B}$ is the position vector pointing from the satellite to the third body, and $\mathbf{r}_{e-3B}$ is the position vector pointing from the Earth to the third body. In this case since we are considering multiple third body contributions (Sun, Moon, and Mars), the respective terms $\mathbf{a}_{3B_i}$ must be summed up together. The solar radiation pressure ($\mathbf{a}_{SRP}$) and the atmospheric drag ($\mathbf{a}_d$) perturbing accelerations can also be added to the dynamical model within $\mathbf{a}_p$ if needed. Particularly, the atmospheric drag is significant for Low Earth Orbit (LEO) applications, whereas the SRP is important for GEO, X-GEO and cislunar applications. In this case, we considered SRP in our model since we are dealing with a cislunar object. The cannonball model has been employed in this work under the assumption of a constant effective area [13]:

$$\mathbf{a}_{SRP} = P_0(1+C_r)\frac{R_0^2}{r^2_{Sun-sat}}\frac{A}{m}\frac{\mathbf{r}_{Sun-sat}}{r_{Sun-sat}} \tag{11}$$

where $P_0 = 4.57 \cdot 10^{-6}$ N/m^2, C_r is the satellite's reflectivity, $R_0 = 149.6 \cdot 10^6$ km is the average Earth-Sun distance, A is the satellite's cross section area seen by the Sun, m is its mass, $\mathbf{r}_{Sun-sat}$ is the vector pointing from the Sun to the satellite and $r_{Sun-sat}$ is the corresponding distance. One important remark is that in case SRP is used in the model, the area-to-mass ratio of the satellite has to be estimated as well, unless it is provided beforehand.

2.2.1 Computed Observables

A model describing the relationship between state and observables has to be defined in order to perform the OD task and to compare the output with the ephemeris of the target. Since the telescopes observations are provided in a topocentric inertial reference frame, the estimated right ascension and declination are:

$$\alpha = \arctan\left(\frac{y_{os}}{x_{os}}\right) \tag{12}$$

$$\delta = \arcsin\left(\frac{z_{os}}{r_{os}}\right) \tag{13}$$

where $\mathbf{r}_{os}(t) = [x_{os}, y_{os}, z_{os}]$ represents the relative position between the observer ($\mathbf{r}_o(t)$) and the satellite, i.e., $\mathbf{r}_{os} = \mathbf{r} - \mathbf{r}_o$, and r_{os} is its magnitude.

It should be noted that, in order to avoid numerical problems related to angles (e.g., indetermination and jumps) and to avoid computing arctan and arcsin, the sine and cosine of the angles are used instead of the angles themselves. Specifically, $\sin\alpha$, $\cos\alpha$, and $\sin\delta$ are used to completely define a direction, thus avoiding the use of actual angles.

3. NUMERICAL RESULTS

The proposed method has been tested two scenarios. Firstly, real observation data has been used to recover the final month of the trajectory of the Chang'e 5 T1 booster before it made impact with the far side of the Moon on 4 March 2022. Secondly, simulated data has been generated starting from the real Chang'e 5 trajectory by applying a fictitious maneuver, which has been used to test the maneuver estimation capabilities of the method.

3.1 Real trajectory estimation

Data for Chang'e 5 T1 is available throughout most of the mission, spanning from March 2015 to February 2022. In this work, we focused on the final part of the mission, from February 2022 to the impact on the Moon happened on March 4th, 2022 at 12:25:23 UTC as predicted by Bill Grey[1] and JPL and subsequently proven by imagery from the Lunar Reconnaissance Orbiter (LRO)[2]. Specifically, the data utilized is composed by 35 observations that span between 01:55:41 UTC and 20:45:02 UTC on 2022 February 8. The observations come from a group of observatories comprising one of Space4 telescopes located at the Biosphere2 in Tucson, Arizona (designation: V17), the Loiano Observatory (Osservatorio Astronomico di Loiano - designation: 598) located in Italy and the Calar Alto-Schmidt telescope (designation: Z84) located in Spain.

The PIOD framework is able to accept observations as a text file using the MPC 80 columns format, which represents a standard for telescope observations, as well as customized text files. In this case we used the MPC 80 column format. All dimensions have been made non-dimensional by introducing the parameters $\bar{\mu} = 398600.1$ km^3/s^2 and $\bar{R}_e = 6378.1366$ km. All other dimensions are made non-dimensional using these parameters. The dynamical model used in this case is the one described in Section 2.2, with the control action turned off. The NN model is based on the ELM definition described in Section 2.1 with number of neuron $m = 30$ and hyperbolic tangent activation function. The input weights and biases for the ELM are randomly chosen from a uniform distribution within the interval $[-1, 1]$. The number of collocation points used to calculate the physics loss is set to $N_f = 100$, while the number of collocation points for the observations are of course equal to the number of observations ($N_\theta = 35$). The parameters λ_f and λ_θ are set to 1.

Figure 1 shows some performance metrics related to this specific problem. On the top left, the observations in terms of right ascension and declination are reported. The top right plot shows the residual between the real and estimated observations, which are quite low (10^{-4}). The accuracy of the OD solution can also be seen from the two bottom plots showing the value of the loss on the physics collocation points and the observation points. The very low physics loss demonstrates that the physics is satisfied by the solution, while the low observation loss shows that the solution matches the observations as well. It should be noted that the loss is shown on the actual observables used in the PIOD method ($\sin(\alpha), \cos(\alpha), \sin(\delta)$) instead of the angles themselves.

Figure 2 shows the estimated trajectory as well as its comparison with the ephemeris obtained using the Horizon System by JPL[3]. The plot on the left shows good overlapping of the estimated trajectory and the ephemeris, which indicates a relatively small error between the two. The small errors in terms of position is also confirmed by the central plot which shows position errors below 4.5 km. The plot on the right shows the propagated trajectory up to the impact with the Moon starting from the point the lowest average physics loss, which was arbitrarily selected as the most accurate estimated state. Figure 3 shows the state error, both in terms of position and velocity, along the estimated trajectory with respect to the ephemeris. This plot contains the entire error information as it shows errors by components at each collocation point. The error on position is greater on average in the X-axis, with the Z-axis being on average the most accurate. The error in velocity is very small, generally below 2 cm/s. Figure 4 shows the comparison of the propagated trajectory shown in Figure 2 and the ephemeris up to the impact with the Moon. This shows that the solution remains close to the ephemeris for the entire duration of the propagation, with errors below 120 km in position. Importantly, the plot on the right shows the angular error along the trajectory with stays within the FOV of one of the telescopes at Space4 capable of recovering this object. This proves that the OD solution could be safely used to track the object and eventually re-observe it in the future. Finally, Figure 5 shows the distance between the spacecraft and the center of the Moon, both for the estimated trajectory and the "real" ephemeris. This proves that the estimated trajectory is capable of predicting the impact with the Moon with good accuracy, further validating the solution.

[1] https://www.projectpluto.com/temp/dscovr.htm
[2] https://www.projectpluto.com/temp/imaged.htm
[3] https://ssd.jpl.nasa.gov/horizons/

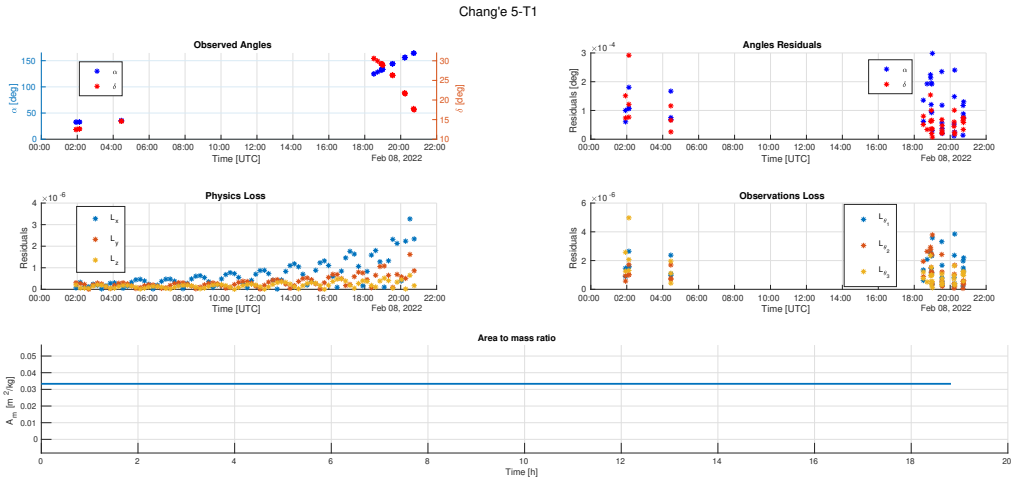

Fig. 1: PIOD performance metrics on Chang'e 5-T1 trajectory estimation.

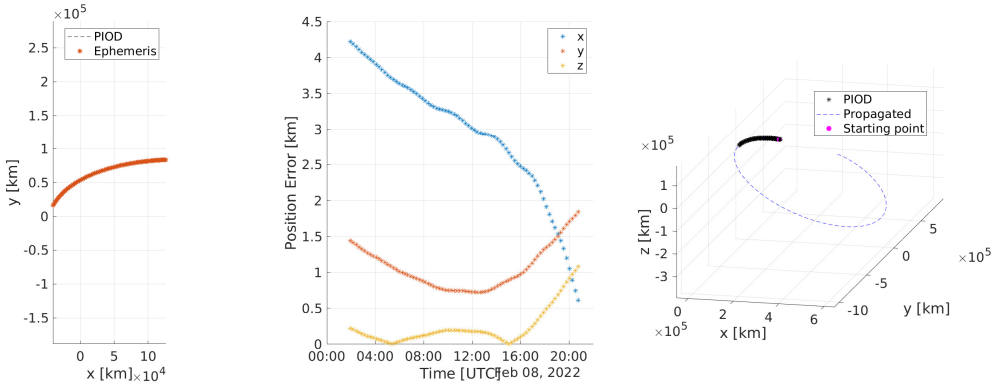

Fig. 2: Estimated trajectory and propagation.

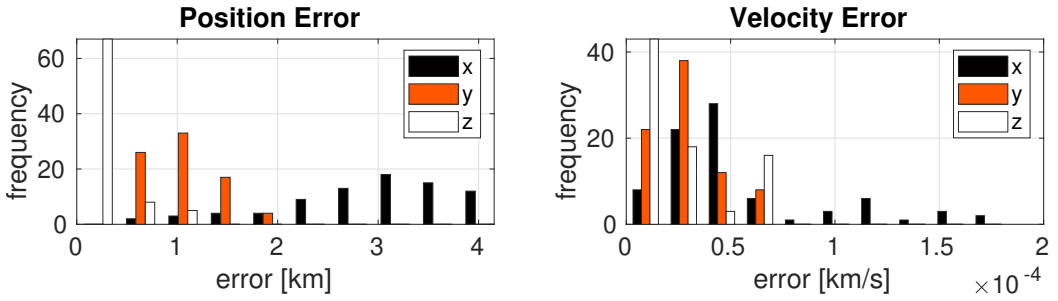

Fig. 3: Errors along estimated trajectory.

3.2 Maneuvering target state estimation

The method is then tested on a simulated trajectory with a control acceleration introduced at some arbitrary interval. The trajectory has been obtained by selecting the initial state from the Chang'e 5-T1 ephemeris at 15 January 2022 18:08:40 UTC. The trajectory is then propagated forward in time using the model described in Section 2.2, adding a continuous arbitrary control acceleration within a specified interval.

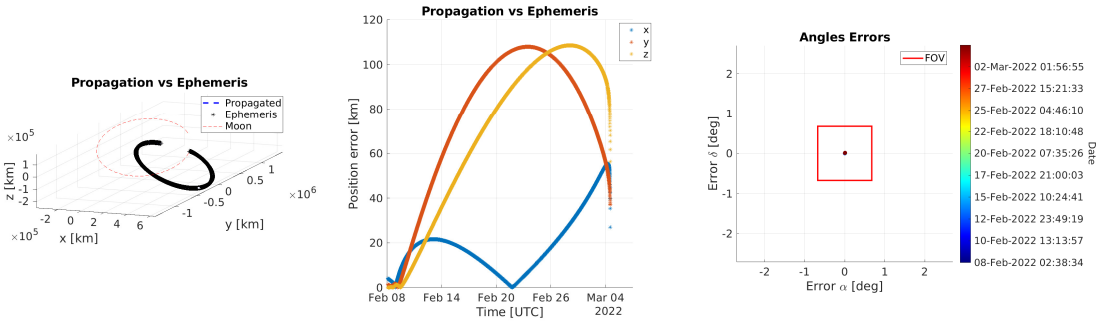

Fig. 4: Estimated trajectory: comparison with ephemeris.

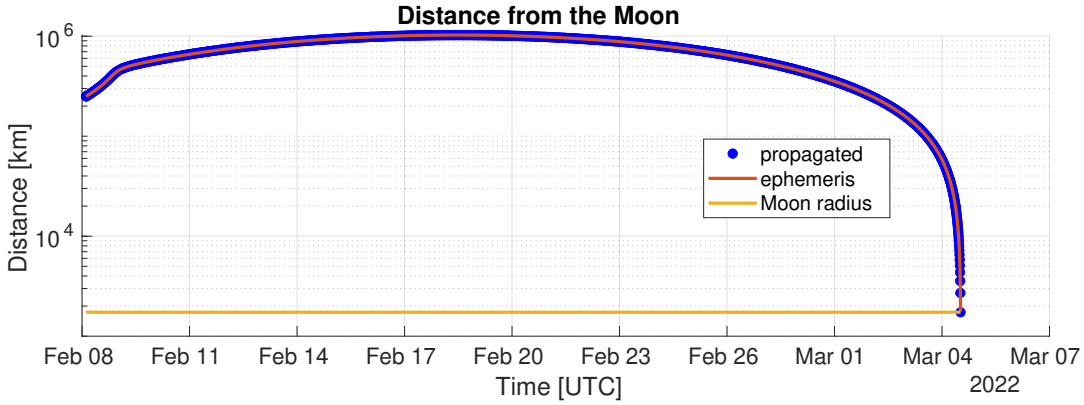

Fig. 5: Distance with respect to the center of the Moon (the impact with the Moon surface is visible at the final time).

In this case, the maneuver is being performed between 17 January 2022 17:27:58 UTC and 18 Jan 2022 17:55:19 with a constant thrust of 20 N (with an assumed spacecraft mass of 4000 kg) aligned with the radial direction. The results are shown in Figures 6-9. Figure 6 shows the trajectory of the spacecraft with and without the control acceleration, as well as the estimated trajectory and the propagated trajectories after the last observation for a period of 6 days. This figure visually shows good agreement between the estimated and real trajectory, even when propagated forward in time. Figure 7 shows the estimated control acceleration versus the real control acceleration. Although the overall shape of the estimated acceleration does not exactly following the real acceleration profile, the location of the control is correctly predicted as indicated by the visible ”bulge” in all components. Moreover, the obtained solution seems to have a higher peak but lower duration, which ultimately results in similar overall total DV. It is worth noticing that, for the purpose of trajectory estimation and orbit determination, retrieving the real control acceleration profile is not crucial, as long as the trajectory is estimated accurately. Figure 8 shows some performance metrics related to the PIOD solution, such as the angle residuals, the physics and the observation losses. Finally, Figure 9 shows the position errors between the propagated trajectory and the real one as well as the angle deviations with respect to the chosen observatory location (Tucson, Arizona). The trajectory is obtained using the estimated state at the last observation as initial state and propagated forward for 6 days. The solution is compared with the real trajectory propagated for the same amount of time. The solution matches the real trajectory within 3000 km. More importantly, the angular error below 0.01 degrees means that the object is within the FOV of most of the telescope at the Space4 Center, which indicates that the solution could be used for follow-up observations. Future and continuous tracking of a space object is ultimately the main motivation behind this work.

4. CONCLUSIONS

This paper presents an application of the recently introduced Physics Informed Orbit Determination (PIOD) to cislunar objects with maneuver detection and estimation. The method employs physics informed neural networks to estimate

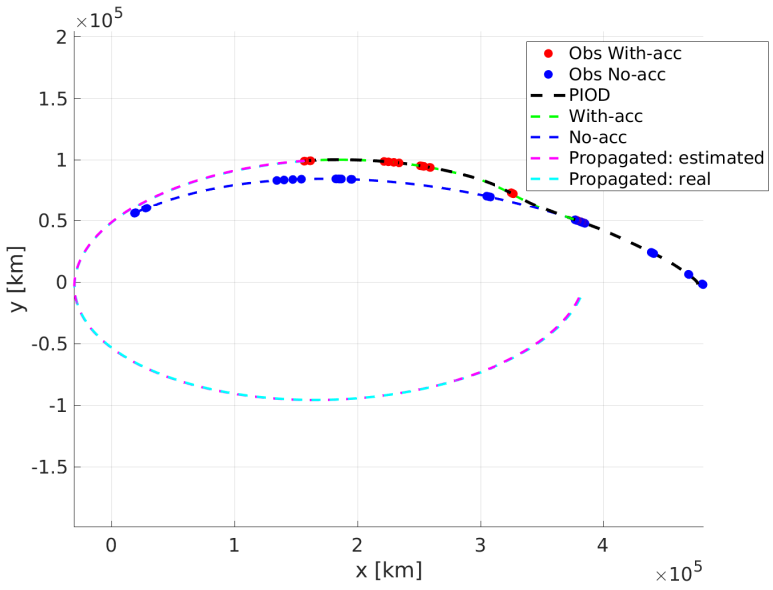

Fig. 6: Estimated controlled trajectory

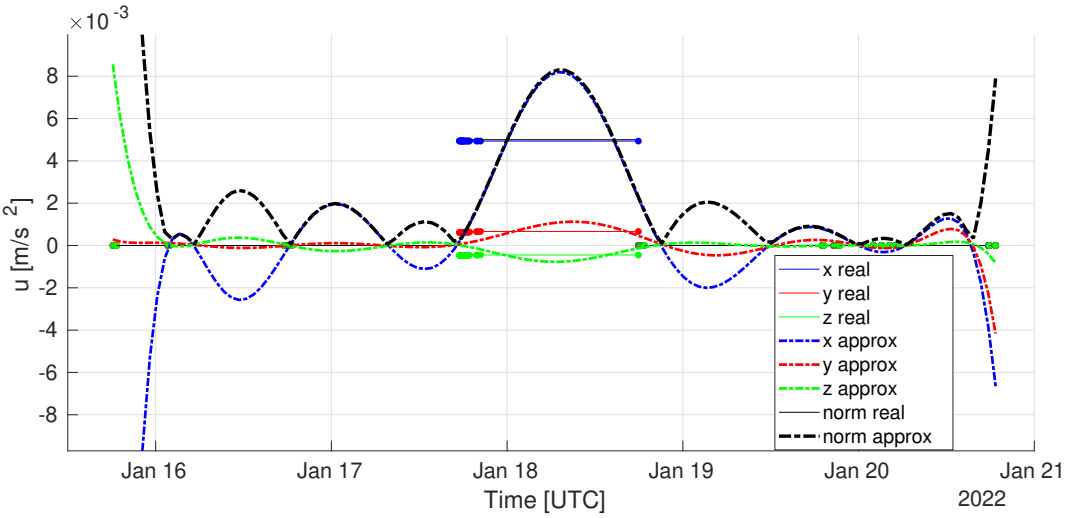

Fig. 7: Estimated control acceleration.

the state of a satellite using angle-only measurements. The equations of orbital motion with zonal (up to J6) and tesseral (J22) harmonics, as well as solar radiation pressure and third body effects are considered. These are used to regularize the network training and ensure that the solution fits both data and physics. The method shows good estimation performance when using real observations of the upper stage of the Chang'e 5-T1 mission. The estimation matches the ephemeris provided by JPL within 4 km in position and 2 cm/s in velocity, which allows for accurate propagation for nearly a month after the last observation until the correcly predicted impact with the far side of the Moon. Moreover, the method is able to estimate an unknown maneuver performed by the observed satellite. The test shows that, although the estimated maneuver doesn't closely match the real one, the estimated trajectory can be effectively used to recover the object with subsequent observations, proving valuable for real world applications.

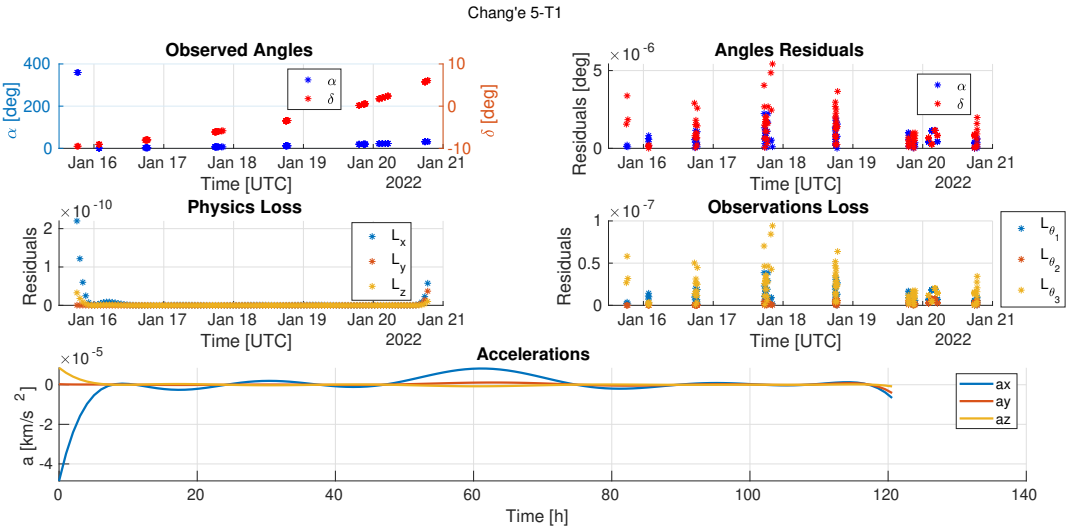

Fig. 8: PIOD performance metrics on controlled trajectory.

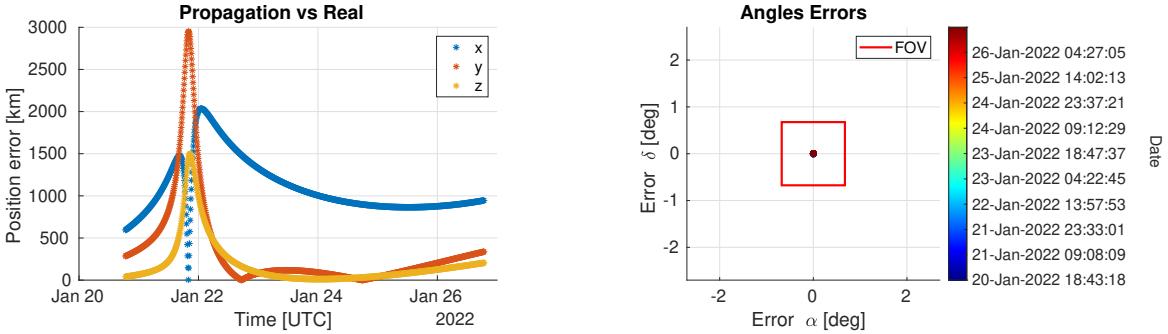

Fig. 9: Position and angular residuals on propagated trajectory.

REFERENCES

[1] Michael R Thompson, Nathan P Ré, Cameron Meek, and Bradley Cheetham. Cislunar orbit determination and tracking via simulated space-based measurements. In *Advanced Maui Optical and Space Surveillance Technologies Conference (AMOS)*, 2021.

[2] Steve Creech, John Guidi, and Darcy Elburn. Artemis: An overview of nasa's activities to return humans to the moon. In *2022 IEEE Aerospace Conference (AERO)*, pages 1–7. IEEE, 2022.

[3] Terry D Haws, Joshua S Zimmerman, and Michael E Fuller. Sls, the gateway, and a lunar outpost in the early 2030s. In *2019 IEEE aerospace conference*, pages 1–15. IEEE, 2019.

[4] Reza Raymond Karimi and Daniele Mortari. Initial orbit determination using multiple observations. *Celestial Mechanics and Dynamical Astronomy*, 109:167–180, 2011.

[5] Bob Schutz, Byron Tapley, and George H Born. *Statistical orbit determination*. Elsevier, 2004.

[6] Andrea Scorsoglio, Luca Ghilardi, and Roberto Furfaro. Orbit determination via physics informed neural networks. In *31st AAS/AIAA Space Flight Mechanics Meeting, Virtual, February 1-3*, 2021.

[7] Andrea Scorsoglio, Luca Ghilardi, and Roberto Furfaro. Orbit determination via physics informed neural networks in cislunar environment. In *2021 AAS/AIAA Astrodynamics Specialist Conference, Big Sky, Virtual, August 9-11*, 2021.

[8] Andrea Scorsoglio, Luca Ghilardi, and Roberto Furfaro. A physic-informed neural network approach to orbit determination. *The Journal of the Astronautical Sciences*, 70(4):1–30, 2023.

[9] Andrea D'Ambrosio, Andrea Scorsoglio, Luca Ghilardi, Roberto Furfaro, and Vishnu Reddy. State estimation with angle-only observations in cislunar space via physics-informed neural network. In *2023 AAS/AIAA Astrodynamics Specialist Conference, Big Sky, Montana, August 13-17*, 2023.

[10] Vikas Dwivedi and Balaji Srinivasan. Physics informed extreme learning machine (pielm)–a rapid method for the numerical solution of partial differential equations. *Neurocomputing*, 391:96–118, 2020.

[11] Guang-Bin Huang, Qin-Yu Zhu, and Chee-Kheong Siew. Extreme learning machine: theory and applications. *Neurocomputing*, 70(1-3):489–501, 2006.

[12] Matthew J Weinstein and Anil V Rao. Algorithm 984: Adigator, a toolbox for the algorithmic differentiation of mathematical functions in matlab using source transformation via operator overloading. *ACM Transactions on Mathematical Software (TOMS)*, 44(2):21, 2017.

[13] Daniel J Scheeres. *Orbital motion in strongly perturbed environments: applications to asteroid, comet and planetary satellite orbiters*. Springer, 2016.